Design and Development of a Closed-Cycle Cryogenic System for Continuous 4 K Operation as a Liquid Helium Alternative

CHAKIB BELGHAIT

Concordia University/John Abbott College

Independent Research Project in Engineering
360-RES-AB (Winter 2025)

Research Supervisor: Valter Zazubovits, Concordia University
Course Coordinator: Ferenc Balogh

May 28, 2025

Contents

Abstract:

This paper presents the design and improvement of a closed-cycle cryogenic system intended to operate continuously near 4 K, as an alternative to liquid helium for spectroscopic studies of various substances including light-harvesting complexes (LHCs) involved in photosynthesis. Studies on LHCs are essential in biophotonics and increasingly relevant to the development of new solar energy technologies and cryogenic systems are beneficial in this research field. The design for our cryogenic closed-system is built around a Sumitomo RDK-415D cryocooler, powered by a 7.5 kW helium compressor. The system uses a thermodynamic cycle where helium gas gets compressed and expands rapidly. The cryostat is protected and placed in a hermetically sealed aluminum vessel under vacuum, and the coldfinger is surrounded by a radiation shield to minimize thermal losses due to radiation. Heat is then transferred from the cold head to the sample chamber through gold-coated copper rods ensuring optimal thermal conduction. The compressor is cooled by running water to maintain stable operation. Manufacturer data and theoretical calculations suggest that the system can reach a base temperature of approximately 3.8 K. With design improvements, a hypothetical lower temperature limit of 2.2 K is possible. Currently, temperature sensor calibration remains a challenge, requiring either access to liquid helium or use pre-calibrated systems. The main goal behind this design is to fully replace liquid helium, which has become both costly and unreliable due to global supply shortages. By offering a sustainable and reusable alternative, this system will support research institutions working in ultra-low temperature environments.

Introduction

With the recent decrease in fossil fuel reserves and the massive increase in climatic issues caused by burning fossil fuels, the need to find a sustainable and renewable alternative to this archaic energy is essential. Naturally, with such an important need world-wide, the amount of research and experiments conducted on this topic is also increasing. Wind, nuclear and hydrogen energy are just a few examples of potential replacements for fossil fuels, however, amongst all, the most research has focused on the utilization of solar energy (Tan *et al.*, 2021). Using the sun's light as an energy source, solar energy is, so far, the most reliable, cost-efficient and sustainable type of energy that would be able to replace fossil fuels (Qiu *et al.*, 2019). One avenue of solar energy research involves exploring natural photosynthesis, and to fully understand and replicate the biological mechanisms that make natural photosynthesis so efficient, researchers must rely on high-precision spectroscopic techniques that often require ultra-low temperatures. This dependence on cryogenic conditions creates a growing need for sustainable cooling technologies, especially as traditional systems like liquid helium become increasingly costly and unreliable.

A lot of research is being conducted on the different ways to convert light energy into electricity. Currently, the photovoltaic effect is the most efficient way to collect and use solar energy, however, a lot of researchers are looking into the biophotonics of photosynthetic organisms (Brudvig *et al.*, 2010, & Zazubovitch & Jankowiak, 2015). This refers to the study of light-based processes and interactions within organisms that perform photosynthesis, particularly focusing on how they absorb, emit, and utilize light energy at the molecular and cellular levels (Lagorio *et al*., 2021). Understanding how certain organisms convert sunlight into energy could lead to a brand-new way of conceiving solar energy panels, most notably with the improvement of the current photovoltaic cells or with the conception of artificial light harvesting technologies that may be even more efficient than what is used today (Brudvig *et al.*, 2010). Research institutions and universities are actively conducting experiments on the light-harvesting complex proteins (LHC) within photosynthetic organisms that capture light and forwards it to the photosynthetic reaction centers where it is converted into chemical energy. To this date, many different kinds of LHCs are being studied for that purpose. Light-

Harvesting Complex II (LHCII), Light-Harvesting Complex I (LHCI) and Fenna-Matthews-Olson Complex (FMO) are just few examples of complexes that are used to explore energy and charge transfer (Croce & Amerongen, 2014). Since the natural conversion of light into chemical energy involves electron transport, this process may be hijacked to produce photocurrent, which is the ultimate goal of artificial light harvesting technologies.

The most efficient technique for studying these complexes is optical spectroscopy, which is a scientific technique that consists of shining light at different wavelengths on a sample to observe how it interacts with light. Optical spectroscopy can reveal a lot of different information about photonics and other spectral properties of a sample, explaining why there are multiple techniques of spectroscopy, each analyzing specific properties. Relating to LHC proteins, many spectral properties are worth studying, which could help improve current solar energy technologies. All photosynthesis complexes display a wide absorption spectrum, and this phenomenon is called inhomogeneous broadening. This phenomenon is caused by small variations in the local environment of the pigment molecules, like chlorophyll, which are embedded in each pigment-protein complex (PPC). While the structure of these complexes is the same across the sample, the local environment around each pigment is never perfectly identical from one complex to another. This leads to identical pigments in the same position to absorb light at slightly different wavelengths, resulting in a broadening of the absorption spectra line (Rätsep & Freiberg, 2007). These variations in local environments are partly visualized by the protein energy landscape, which refers to a conceptual map of all the slightly different shapes, or conformations, the LHC protein can adopt. As the protein fluctuates through different conformations, either functionally (e.g. switching between light-harvesting and photoprotective states) or randomly, the structural changes around the pigment molecules influence their spectral properties, further contributing to inhomogeneous broadening (Chmeliov et al., 2016).

This phenomenon of inhomogeneous broadening and this theoretical model of the energy landscapes among other spectral properties are studied as they can give precious insight on light absorbance under low-conditions and how to design adaptive and self-regulating systems capable of doing what is observed in LHCs. To examine these

properties, optical spectroscopy is required, but, more specifically, researchers use a specific spectroscopic technique called spectral hole burning (SHB) that can isolate a specific fraction of the molecules of the pigments they want to focus their attention on (Chmeliov *et al*, 2016). SHB is conducted as follows: after measuring an absorption spectrum, where inhomogeneous broadening is displayed, a narrowband laser, calibrated at a fixed wavelength, will excite all the molecules that can absorb this exact wavelength, causing these molecules to change frequency and shift in the spectrum creating a "hole" in the absorption spectrum. The researchers then observe this hole during a long period of time to see how the molecules are reacting. This close monitoring will help understand some of LHC's spectral properties like protein dynamics and energy relaxation (Rätsep & Freiberg, 2007).

A requirement of the SHB technique is to cool the sample to very low temperatures in order to reduce the thermal broadening of the spectral lines. To have a clear view of what is happening, it is necessary to minimize any thermal motion. This is where cryotechnologies come into play. To reduce the kinetic energy of the sample, it must be held at temperatures approaching absolute zero (0 K or -273.15ºC), at which there is no longer any trace of motion and kinetic energy is present. However, this is just a theoretical temperature that can be approached but never reached (Mokbel *et al,* 2024). To reach such low temperatures, also called cryogenic temperatures, the use of a cryogenic cooling system is required. For the past decades and still today, the most used cryogenic coolant is liquid helium, as helium is the element with the lowest boiling point (4.2K or -268.95ºC). However, helium is a non-renewable resource, formed by radioactive decay underground and extracted as a byproduct of natural gas. This means that the amount of available helium in the world is very limited. This, combined with the increase in the amount of research requiring these cryogenic temperatures (as well as use of MRI machines with cooled superconducting magnets for medical purposes), causes a massive increase in demand while maintaining a decrease in offer. This resulted in the price of liquid helium to skyrocket, passing from 7.50$/L to 60$/L in Montreal (Nordum, 2024.). For many research institutions, investing in liquid helium as their cryogenic cooling system is no longer possible, and the few still using it have rising concerns about long-term availability. Not a lot of alternatives exist and few of them are as efficient. The most promising replacement are cryocoolers. They function by using helium gas and

through a series of thermodynamic cycles, expand it to reach similar temperatures. Although cryocoolers already exist, they remain in limited supply and are produced by only a few companies, making them expensive and difficult to access. A promising alternative is the use of mechanical cryogenic systems that rely on helium gas in a closed-loop, eliminating the need for refills while still reaching very low temperatures. Designing and building a reusable, closed-cycle cryocooler offers a more sustainable and accessible solution. The conception and implementation of such a system is the focus of this paper.

Design and Methods

Overview:

This section will review the mechanical design and configuration of each part of the cryogenic closed-system. The system is composed of four main sections: the helium compressor unit, the cooling unit, the observation setup and the thermal management.

Helium Compressor Unit:

The Sumitomo CSW-71C helium compressor unit is the initial component of this cryogenic closed-system, feeding high-pressure helium gas to the remaining components. The compressor closed-system starts by receiving low-pressure helium gas from the cryocooler (1) at pressures around 1.60 to 1.65 MPa. This gas passes through a storage tank (2) and filter system (3) designed to remove any contaminants before reaching the compressor capsule (4). In this capsule, the gas will undergo mechanical compression, making it reach high pressures ranging between 2.00 and 2.20 MPa. By the First Law of Thermodynamics, this sudden compression will increase the gas's temperature. This hot and pressurized gas is then conveyed through a helium gas cooler (5), which is a water-cooled heat exchanger that reduces the gas temperature through conduction while minimizing the lowering of the gas pressure. Following the cooling phase, the gas enters an oil separator (6), where the oil mist introduced during compression will be removed. This collected lubricating oil is directly recycled back into the compressor capsule. The helium gas is then driven through an active charcoal layer (7) to remove any other oil traces, assuring a high purity level in the gas supply. The power of the compressor is approximatively 7.5kW. The purified helium is then delivered to the cryocooler through two specialized high-pressure flexible helium lines: a supply and a return line (8, 9). The helium compressor operates within a fully sealed closed-loop system, preventing any helium gas loss and allowing continuous operation with the machine. Additionally, a water-cooling system composed of two water lines (10, 11) has also been installed to maintain stable performance and prevent the compressor from overheating.

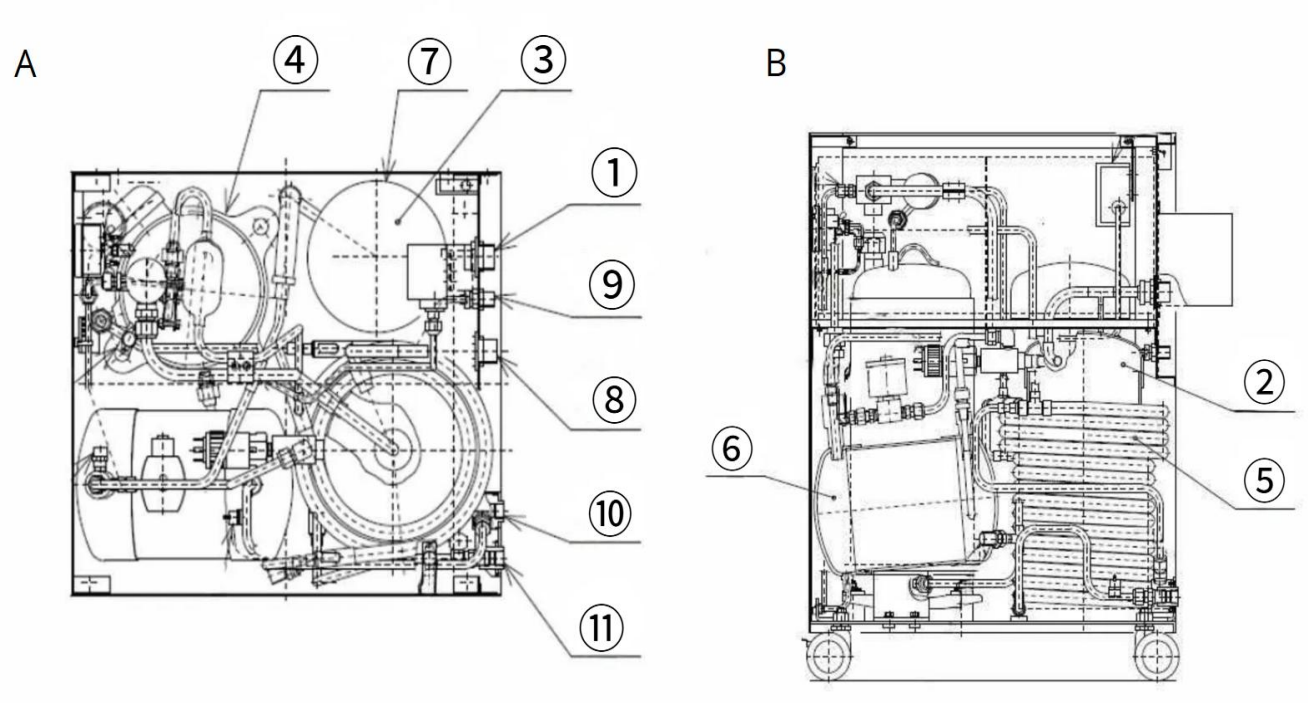

Figure 1. Internal component layout and schematic diagram of the Sumitomo CSW-71C. Top view (A) of the helium compressor shows the helium gas return connector (1), the filter (3), the compressor capsule (4), the adsorber (7), the helium gas supply (8) and return (9) connector and the cooling water inlet (10) and outlet (11). The side view shows the storage tank (2), the helium gas cooler (5), and the oil separator (6). All labels and numbering were added by the author for clarity. *(Adapted from Sumitomo Heavy Industries, Ltd., CSW-71C Compressor Unit Technical Instruction Manual, 2009)*.

Cryogenic Cooling Unit:

Overview

The setup continues with the Sumitomo RDK-415D 4K cold head, which takes the role of the principal cryocooler for the entire system. This cold head is part of Sumitomo's SRDK series and this model in the series and was chosen because it was the unit with most past history among the cryocoolers available on eBay for reasonable price, giving us enough data to consider a high chance of good functioning. Directly connected to the helium compressor, it receives high-pressure helium gas , which will undergo

controlled expansion and cooling. The cryocooler uses the Gifford-McMahon (GM) cycle, which relies on helium gas being compressed and expanded in a closed-loop. Internally, the RDK-415D is composed of 3 main sections: the drive unit, the displacer–regenerator unit and the cylinder unit.

The Gifford-McMahon Cycle:

The Gifford-McMahon (GM) cycle is the refrigeration process that allows the cryocooler to reach these very-low temperatures without consuming any liquid cryogens, like liquid helium. It works by compressing and expanding helium gas periodically in a closed-loop. The high-pressure helium enters the cold head through a rotary valve (10) and is directed into the regenerator (14,15), where it will be precooled by the previously cooled helium still present. The gas then gets mechanically expanded in a low-pressure area of the cryocooler. By the First Law of Thermodynamics, this rapid expansion will cause a major temperature drop, which will automatically enable the heat extraction process from the system's cold stages. The cycle is completed as the cold and low-pressure helium leaves the cryocooler and returns to the helium compressor. This periodic thermodynamic cycle of the helium gas keeps the system cold and allows the performance of operation over long periods without losing any gas.

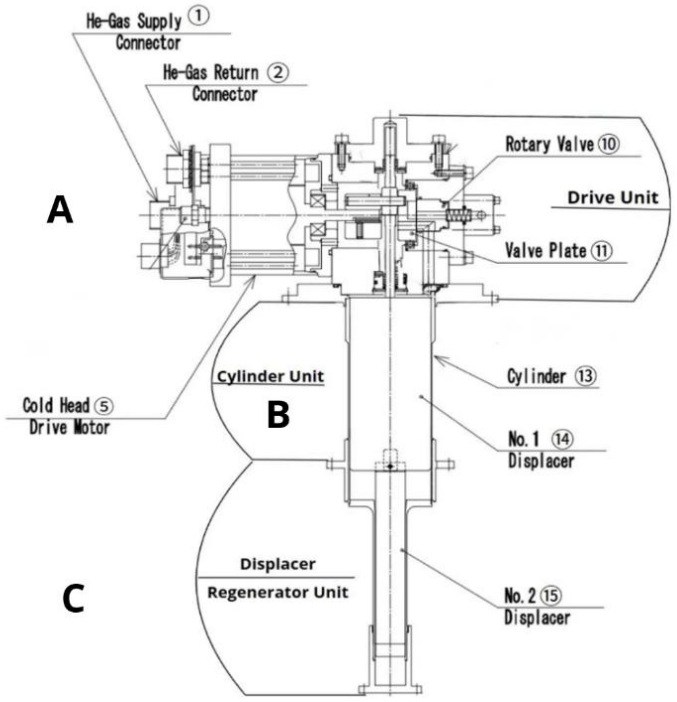

Figure 2. Annotated cross-sectional schematic of the Sumitomo RDK-415D cold head, showing its three main internal sections. At the to top there is the Drive Unit (A) composed of the helium gas supply (1) and return connectors (2), the rotary valve (10), the valve plate (11) and the drive motor (5). In the middle there is the Cylinder Unit (B) made of the Cylinder (13) and the first displacer (14) and composes the first cooling stage. The bottom part is the Displacer–Regenerator Unit (C), which is composed of the second displacer (15) and the regenerator that is within it. It also delimits the second cooling stage. Labels and numbering were added by the author for clarity. This diagram is based on the internal structure of the RDK-205D model, which shares the same architecture with the RDK-415D. *(Adapted from Sumitomo Heavy Industries, Ltd., Cryocooler Technical Instruction Manual: RDK-205D, 2005.)*

Drive Unit:

The drive unit is the first of the 3 main sections of the cryocooler. It is located at the top of the RDK-415D and contains a three-phase AC induction motor (5) and a rotary valve (10). The motor is responsible for mechanically moving the displacer in a vertical reciprocating motion (up and down oscillation). In parallel, it also rotates the rotary valve at a constant speed, which allows the control of the intake and exhaust of the gas. The valve also connects the cold head to the high-pressure receiving line (1) and the low-pressure returning line (2). This allows the rotary valve to control and regulate the gas

flow through the whole GM cycle. The drive unit, through its synchronization of the valve's operation with the displacer's reciprocating motion, ensures that the Helium gas is compressed and expanded at the right moments. This also initiates the thermal exchange that leads to the rapid cooling.

Cylinder Unit:

The cylinder unit forms the central body of the cold head, acting as a pressure chamber (13) in which the helium gas is expanded or compressed, depending on the current phase of the GM cycle. Inside this chamber, the helium flows through some internal channels that direct it throughout the whole cryocooler. This part is also the space where the displacer (14,15) moves up and down. When the helium enters the cylinder, it undergoes a controlled pressurization or expansion depending on which phase of the GM cycle it is at. The cylinder unit is also where the temperature difference between the two cooling stages appears. The top stage stays at a higher temperature, approximately between 40K and 50K, depending on the operating conditions, while the bottom part will theoretically cool down to approximately 4.2 K.

Displacer-Regenerator Unit:

The displacer–regenerator unit is the core of the cryocooler's two-stage cooling mechanism. It consists of a piston (14,15), known as the displacer, filled with a porous metallic material called the regenerator. As helium gas flows through this matrix, the regenerator absorbs heat from the incoming high-temperature gas and releases it back to the returning cold gas, functioning as a heat exchanger. The RDK-415D cold head uses a two-stage regenerator design. The first stage (14) is composed of conventional materials like bronze wire mesh and reaches temperature around 40 to 50 K. The second stage (15) uses rare-earth alloys, most probably $HoCu_2$ or ErNi. These materials are specifically chosen for their high heat capacity at very low temperatures which can allow cooling down to approximately 4.2 K or below. As shown in the figure, common materials like lead (Pb) rapidly lose their heat capacity below 10 K, limiting older cryocoolers to higher base temperatures (9 K). In contrast, rare-earth alloys retain high specific heat near 4 K, enabling the RDK-415D to potentially reach temperatures as low as 2.2 K under ideal operating conditions.

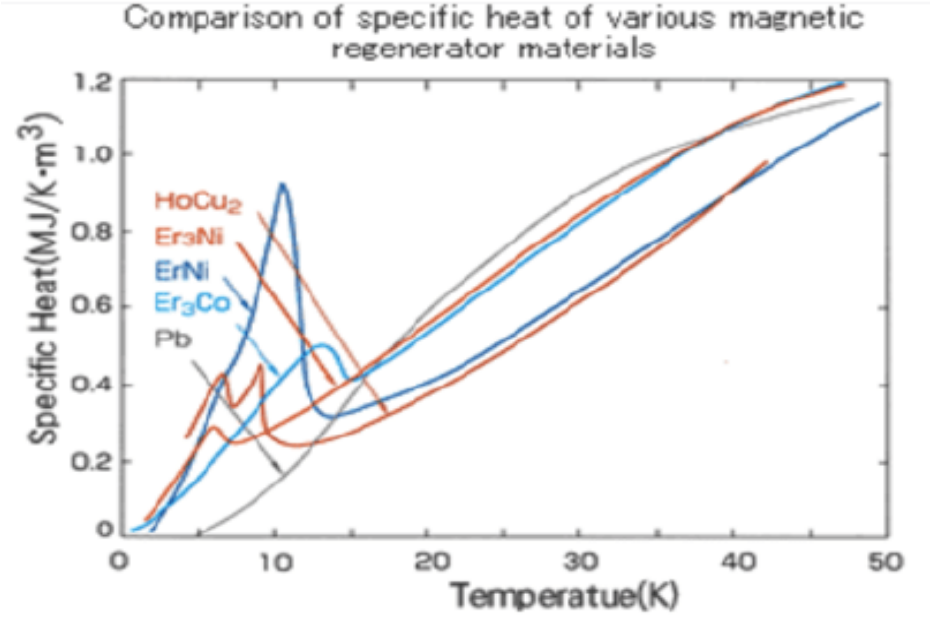

Figure 3. Comparison of the specific heat capacities of various magnetic regenerator materials as a function of temperature. Rare-earth alloys such as $HoCu_2$ and ErNi exhibit sharp peaks in specific heat between approximately 6 K and 8 K, reaching values around 0.9–1.0 MJ/(K·m³). In contrast, conventional materials like lead (Pb) fall below 0.1 MJ/(K·m³) in the same range. This thermal behavior makes rare-earth materials significantly more effective for second-stage regeneration in the cryocooler.

Observation Setup:

Sample Chamber:

The sample chamber is a cubic aluminum enclosure designed to house permanently mounted protein film samples under high-vacuum and cryogenic conditions. The interior of the chamber is thermally connected to the second stage of the cryocooler via a gold-coated flexible copper braid that extends from the copper rod, ensuring efficient conduction of the heat to the sample. The sample is placed in a gold-coated copper plate, fixed in the center of the chamber. This plate is supported by two vertical G10 fibreglass pillars that minimize thermal conduction. Additionally, eight G10 pillars, distributed around the base, isolate the sample platform from the surrounding aluminum

body, which ensures structural support due to its low thermal expansion factor. The upper section of the chamber features a cubic optical head, rotated 45 degrees to the lower section, equipped with two aligned fused silica windows, allowing laser input and output across perpendicular paths. The chamber is housed in a separate vacuum space, distinct from the cryocooler's radiation shield, and is pumped through a lateral port seen on the chamber's outside body. This design allows the sample to be maintained at ultra-low temperatures with minimal thermal loss for long periods. This is ideal for optical experiments such as spectral hole burning (SHB), which may require uninterrupted observations lasting up to a month.

Laser Setup:

The laser used for optical experiments conducted on the LHCs operates in the visible spectrum range and is delivered in free space. The beam of light is shone on a highly-reflective mirror, which deflects it toward the sample chamber. The beam then passes through the sample. Along that axis, on the other side, a series of optical lenses are positioned to collect and analyze the absorbance of the sample. This fixed-path configuration allows stable optical access across the chamber. Multiple laser wavelengths may be used, depending on what spectral properties of the LHC are being studied, and the system is optimized for long-term, high-precision studies requiring uninterrupted optical alignment over a long time.

Temperature Control and Insulation:

Thermal Management:

In order to use the cryocooler to perform optical experiments, it must be connected to the sample in a manner that facilitates cooling (removal of heat that is constantly leaking into the sample from its mechanical support as well as from optical experiment) and minimize vibrations.

To efficiently convey the heat and minimize any unwanted heat transfer along the way, the thermal links are composed of high thermal conductivity elements, like copper. Copper (oxygen-free copper 101) rods were used as a rigid heat conductor between the sample chamber and the cryocooler's cold head, due to copper's high thermal conductivity and structural support. A flexible thermal link composed of braided copper strands was also added at the end of the rigid rod to provide mechanical flexibility and reduce the transmission of vibrations. To further improve the thermal management, the thermal links were gold-coated via electrolysis using an unknown solution that does not contain cyanide. This process prevented copper from oxidising and reduced thermal contact resistance of the thermal links. In the sample chamber, two cooper wires were installed, wrapped around the G10 fiberglass, that power a small resistor-heater attached to the sample cell. This was done in order to control the temperature the sample is exposed too, giving a better control on the system.

System Insulation:

To minimize any heat transfer, several insulating components were used. Radiation shields were installed to completely enclose and protect the second stage of the cryocooler, the thermal links conducting the heat, and the core of the sample chamber. These three radiation shields are all connected forming one big shield which starts at the first stage of the cryocooler, making the whole insulating system stay at 40 K to 50 K. All the protected parts mentioned previously are fully sealed under vacuum within the radiation shield to limit any heat transfer by radiation and convection. According to the Stefan–Boltzmann law, radiative heat transfer increases with the fourth power of temperature. This makes room-temperature surroundings a significant source of heat load and therefore a danger to the preservation of the cryogenic temperature. The shield intercepts this radiation before it can reach the colder internal components, such as the second stage and the sample interface. This same radiation shield continues and extends outward to also enclose the thermal links between the cryocooler and the sample stage, preventing heat loss by radiation. Finally, structural supports inside the sample chamber, made of G10 fibreglass, were installed. G10 is a very low thermal conductivity material that allows mechanical stability without much conductive heat loss. Based on the Law of Thermal Expansion, at colder temperatures, objects decrease in volume, and because of

its low coefficient of thermal expansion, G10 allows the sample chamber to not move when the temperatures drop, which is crucial for the good unfolding of the experiments. The overall structure of our optical cryogenic system was inspired by commercially available system from Montana Instruments (*Montana Instruments*).The price of the most basic version of such cryogenic system is 85,000 USD. Less expensive (~50,000 USD) systems by other suppliers have much higher vibration levels. There are also more expensive systems, for instance the ones proposed by AttoCube.

Results and Discussion

Thermal Performances:

After testing the system, the cooling time to the minimum operating temperature took approximately one hour. The cooling profile was not linear, rather, it started at a slow and constant rate before having an acceleration (steeper) during the mid-phase and slowing down again as the system approached its base temperature. On the best-performing day, two independent sensors recorded minimum temperatures of 2.2 K and 5.5 K, respectively. Both sensors used were silicon diodes, however, their mounting conditions differed. Silicon diode sensors measure temperature by detecting the voltage drop across the diode, which decreases as temperature decreases. Silicon diode sensors measure temperature by detecting the voltage drop across the diode, which increases as temperature decreases due to increasing resistance. However, individual sensors can deviate slightly from the manufacturer's calibration curve. In our case, the sensor came with calibration data at 0 °C, 77 K, and 4.2 K, which suggests it tends to underreport temperature by about 0.5 K to 0.7 K in the low-temperature range. Therefore, the recorded 2.2 K is likely an underestimate, and the actual temperature was probably closer to 2.9 K. Anyhow, due to the multiple improvements, the results strongly suggest that the system is capable of reaching temperatures at or below the specified 4.2 K limit. The more reliable sensor was specifically selected for its thermal connection properties and was in direct contact with the cold stage. The second sensor, potentially encased in plastic, was reused from an older liquid helium cryostat because that may have had poor thermal contact, leading to less accurate readings. These results, while not yet definitive, demonstrate that the system performs within the expected cryogenic conditions and has the potential to reach lower temperatures with further optimization of sensor placement and thermal contact.

Materials Selection:

OFHC Copper:

To reach these very low temperatures, the choice of each material is important to minimize any heat loss and maximize thermal conduction. The thermal links are made of oxygen-free high-conductivity (OFHC) copper, a material chosen for its excellent thermal and electrical conductivity and favorable mechanical. The copper used also has a residual resistivity ratio (RRR) of approximately 200, meaning that the copper has few impurities and defects. This high purity allows a high thermal conductivity (k) and contributes to a high thermal conductance (G), which refers to how well a specific part conducts heat. For the copper rod, the thermal conductance was estimated using the equation: $G = \frac{kA}{L}$, where G is the thermal conductance in W/K, k is the thermal conductivity in W/m·K, A is the cross-sectional area ($1.54 \cdot 10^{-4}\ m^2$), and L is the rod's length (0.152 m). Based on the graph in Figure 4, the copper's conductivity is around 2000W/m·K (RRR ≈ 200 at 6 K), resulting in a conductance of 2.03 W/K. This high thermal conductance is very beneficial for the system as it prevents a limitation in heat flow. If a temperature difference of 3 K is applied across the rod, it would result in a heat flow of 6.08 W, as predicted by the linear form of Fourier's Law: $Q = G\Delta T$. This shows that the thermal links are capable of transporting more heat than what is typically generated during the cryogenic operations. This level of thermal transport confirms that the copper is not the limiting factor in the system's performance. Instead, heat transfer constraints come from the contact resistance at junctions. To limit this and improve surface durability, some parts of the copper thermal links were gold-coated using potassium dicyanoaurate ($KAu(CN)_2$) via electrolysis. This gold coating minimizes surface oxidation, which, by the same occasion, maintains the purity level of the copper. It also improves the thermal connection between the copper and adjacent components, allowing the system to use more effectively the copper's natural high conductance.

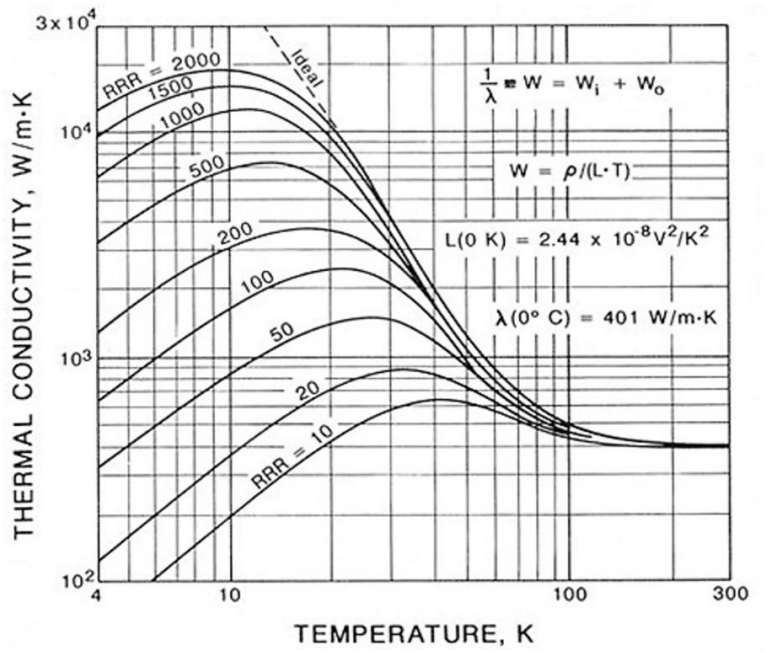

Figure 4. Thermal conductivity of copper at different Residual Resistivity Ratio (RRR) values, from 10 to 2000, as a function of temperature in K. The graph reveals that copper with a higher RRR, indicating a greater purity, shows significantly better thermal conductivity at lower temperatures. For example, copper with an RRR of 200 reaches a thermal conductivity of roughly 2000 W/m·K at 6 K. The graph also reveals that for all RRR values, conductivity peaks between 10 K and 20 K before decreasing at higher temperatures due to the increased phonon scattering. This behaviour reinforces the use of high-purity copper in cryogenic systems, where efficient heat transport is essential to maintain low temperatures across the thermal links.

G10 Fiberglass Epoxy:

The structure of the sample chamber was made using G10 fiberglass epoxy, a material carefully chosen for two key properties: its low thermal conductivity at cryogenic temperatures and its low thermal expansion. These properties allow thermal isolation and mechanical stability in the sample chamber design. G10 fiberglass is one of the weakest thermal conductors across the entire temperature range (See Figure 5). To quantify this effect, we modelled the conduction through four 2.5-inch-long G10 rods of ¼-inch diameter, which suspend the copper plate in the sample chamber. Using the conductivity at 4 K, which is approximately 0.2 W/m·K, a temperature gradient of 36 K (between the 40 K first stage and 4 K second stage), a total cross-sectional area of

$1.23 \cdot 10^{-4}$ m², and Fourier's Law of Heat Conduction ($Q = \frac{kA\Delta T}{L}$), we were able to estimate a heat leak of approximately 0.021 W. This value represents less than 1% of the total heat transport capacity of the copper links (2.45 W), which allows the G10 to be in direct contact with the sample without heating it, and most importantly, it prevents any limitation in heat flow in the design.

G10 is also a key part in maintaining the mechanical structure of the whole sample chamber. According to the Law of Thermal Expansion, every object expands at high temperatures and contracts at low temperatures. As shown in Figure 6, G10 contracts way less than most materials. The glass fibres within the composite strongly contribute to suppressing the shrinkage along the rod axis (normal direction), reducing stress at important joints like the copper-to-G10 junction. This prevents misalignment or cracking during cooldown, maintaining a precise geometry for the optical alignment. Based on that, G10 fiberglass epoxy was chosen for its excellent insulating properties and capability to mechanical stability at low temperatures. These characteristics makes the composite material ideal for structurally supporting the sample chamber without interfering with heat management or alignment.

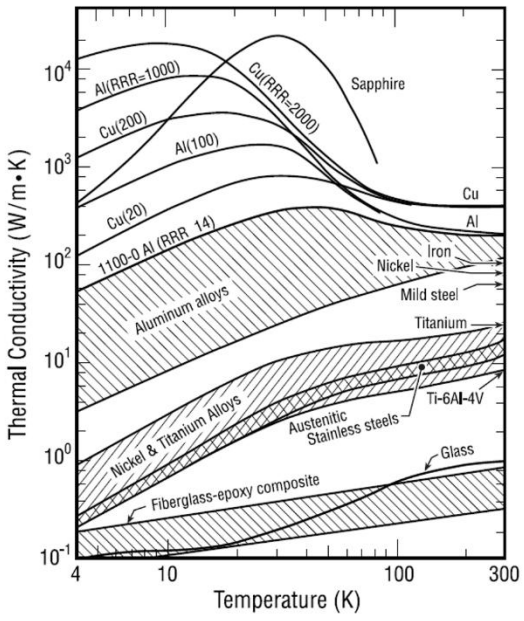

Figure 5. Thermal conductivity (k) in W/m·K for multiple materials used in the design at temperature ranging from 4 K to 300 K. Fiberglass-epoxy composite represents the globality of Fiberglass composites materials in which we can find G10 fiberglass epoxy. According to graph, at 4K, G10 has a thermal conductivity of approximately 0.2 W/m·K.

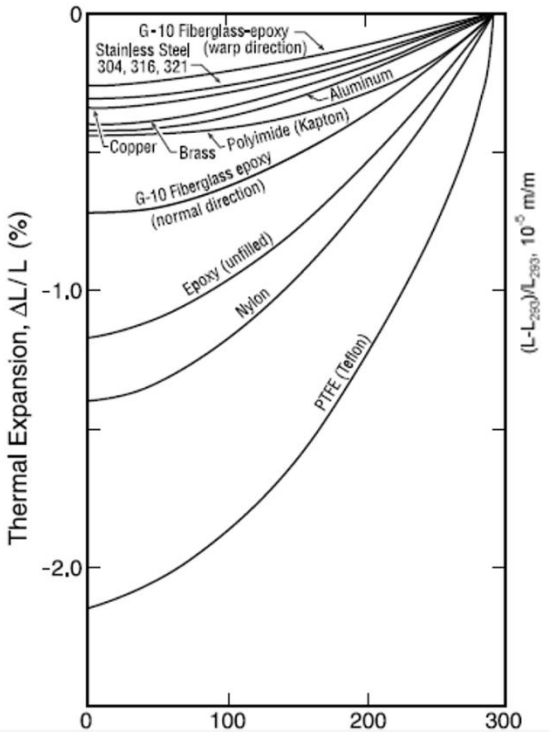

Figure 6. The percentage of change in length of different type of materials, due to thermal expansion, at temperatures ranging between 0 K to 300 K. The G10 fiberglass epoxy's change in length is different at the plane axis/x-y axis (wrap direction) and though thickness/z-axis (normal direction). This difference is due to how G10 is made, which is by layering glass fibers and bonding them with epoxy. The normal direction is mainly dominated with epoxy, which has a higher CTE. While the wrap direction is mainly influenced by the glass fibers with a very low CTE.

Aluminium Alloys:

Most of the system's structural elements, including the radiation shield, are made of aluminum. In cryogenics engineering, there are two main types of alloys: Aluminum 6061-T6 and 6063-T5. Al 6063-T5 was chosen for the radiation shield mostly because of its high thermal conductivity in the low temperature range. The thermal conductivity of Al 6063-T5 reaches a peak of approximately 275 W/m·K around 50 K, significantly outperforming Al 6061-T6, which only reaches about 60 W/m·K at the same temperature. This high thermal conductivity is very beneficial for the radiation shield as it allows it to rapidly distribute the absorbed thermal radiation across its surface and conduct it rapidly towards the first stage of the cryocooler, which stays at around 40 K to 50 K. By doing so, it minimizes hot spots and ensures that the majority of radiative heat is intercepted and dissipated before reaching the second stage, which goes down to below 4.2 K. This thermal management strategy significantly reduces the heat load on the second stage, helping it maintains the cryogenic temperatures. Because the radiation shield is placed under vacuum, heat transfer through convection and conduction is negligible, making heat transfer by radiation the only way of losing heat. This is seen by the Stefan–Boltzmann law:

$$Q = \sigma \epsilon A({T_{Hot}}^4 - {T_{Cold}}^4)$$

Where:

- σ is the Stefan–Boltzmann constant ($5.67 \cdot 10^{-8}\ W/m^2 \cdot K^4$)
- ϵ is the emissivity of the shield material,
- A is the surface area in m^2,
- T_{Hot} and T_{Cold} are the temperatures of the warm surroundings and the shield, respectively.

Assuming an emissivity of 0.1, a surface area of 0.0215 m², and temperatures of 50 K at the shield and 300 K surrounding the shield, the estimated heat intercepted is 0.99 W. This result shows the importance of the radiation shield in limiting the heat entering the cryogenic region. Because aluminum 6061-T6 is more common and costs less, every part not requiring high thermal conduction, like the aluminum vessel enclosing the cold head under vacuum, was made of this material.

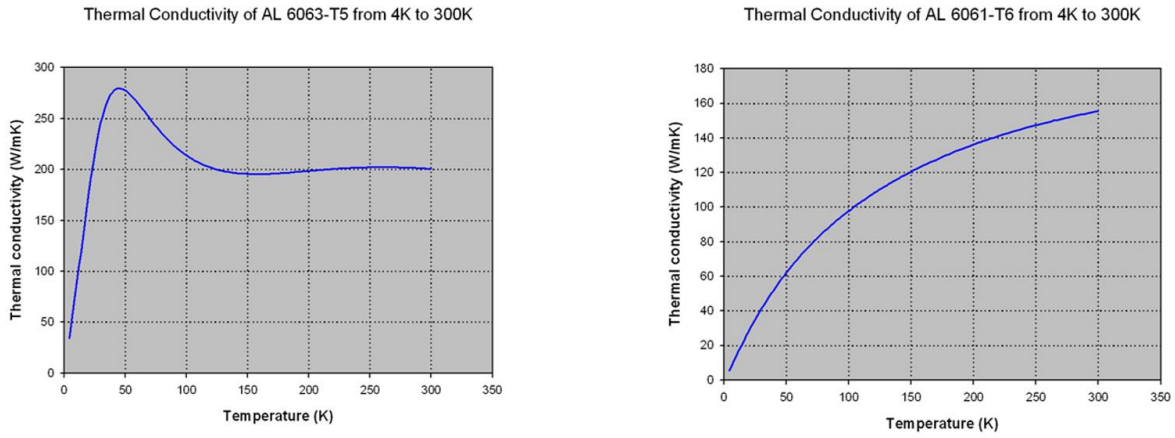

Figure 7: Comparison of the thermal conductivity, in W/m·K, of Aluminium 6063-T5 and Aluminium 6061-T6, from 4 K to 300 K. The graph on the left shows the thermal conductivity of Al 6063-T5, which increases rapidly from 4K to 50K, where it peaks at 275 W/m·K, before slowly reaching 200 W/m·K at 100 K and staying constant at this value. Al 6061-T6, as shown in the graph on the right has thermal conductivity increasing gradually until the end.

Design Improvement:

Multiple design modifications were introduced to improve the performance, stability, and control of the closed-system. First, the radiation shield was installed to prevent heat from reaching the cool temperatures, maintaining the second stage of the cold head and the thermal links at cryogenic temperatures. This change significantly improved the dissipation of radiative heat intercepted at the first stage. Another improvement made to minimize heat loss was to gold coat the flat surface at the bottom of the cold head. While indium was initially chose as the unique interface material, mainly due to its high malleability and thermal conduction, it was later accompanied with

gold due to oxidation and reliability concerns. Indium will still be present between some surfaces to fill irregularities and improve thermal contact. Improvements were also made to ensure a good mechanical structure. For example, because the cold head is powered by two coaxial pistons, a lot of vibration is produced. To reduce the effects of these mechanical vibrations on the system and reduce noise coupling between the cryocooler and the optical table, two stainless-steel bellows were installed. One bellow connects the sample chamber to the outer aluminum vessel, which encloses the cryostat and radiation shield, allowing the copper thermal links to pass through while isolating vibrations. The second bellows is mounted on the opposite side of the vessel, directly connected to the optical table. This two-point configuration ensures mechanical decoupling in both directions and prevents the propagation of the vibrations to the sample and to the optical instruments. However, the primary role of a such setup and the second bellow is to ensure symmetrical contraction when vacuum is created. To have better control over the temperature at which the samples are exposed, a heater was integrated into the sample chamber. The heater consists of a small resistor attached to the sample film and powered by two copper wires wrapped around a G10 fiberglass pillar, where current passes, producing resistive heating. This setup allows localized warming for the protein film samples, allowing experiments that require a temperature higher than the temperature reaching the sample chamber. These modifications improved the system's thermal management and mechanical isolation, which means that the system could hypothetically reach temperatures below the 4.2 K expectations.

Conclusion

The cryogenic closed system presented in this paper, which was designed to replace liquid helium, managed to achieve temperatures between 5 K to 2.9 K, which is significantly below what was predicted. The system consists of a Sumitomo RDK-415D cryocooler with a low-emissivity aluminum radiation shield, high-purity copper links, and G10 fiberglass structural supports. For better mechanical stability, two stainless-steel bellows were installed. A resistor-heater was also added for more precise temperature control at the sample. Further improvements on the sensors' calibration could be made to ensure higher precision for the test results. Conclusively, the system showed reliable performances and a capability for advanced spectroscopic experiences on various LHCs.

Acknowledgments

I would like to thank Professors Jason Lapointe, Zoe Solomon Baird, and Ferenc Balogh for their invaluable guidance, feedback, and support throughout this research. I would also like to express my gratitude to Concordia student Marine Hottelet, graduate students Alexander Levenberg and Milad Babaei along with Dr. Valter Zazubovits for their contribution and involvement during the entirety of this research project.

References

Chmeliov J., Gelzinis A., Songaila E., Augulis R., Duffy C.D.P., Ruban A.V., Valkunas L. The nature of self-regulation in photosynthetic light-harvesting antenna. *Nature Plants.* Vol. 6. 2016

Croce, R., Van Amerongen, H. Light-harvesting in photosystem I. *Photosynth Res. Vol*.116**.** p.153-166. 2013

Croce R, van Amerongen H. Natural strategies for photosynthetic light harvesting. *Nat Chem Biol.* 10(7): 492-50. 2014

De Wit M., Welker G., Heeck K., Buters F.M., Eerkens H.J., Koning G., van der Meer H., Bouwmeester D., Oosterkamp T.H. Vibration isolation with high thermal conductance for a cryogen-free dilution refrigerator. *Rev. Sci. Instrum.* 90 (1). 2019.

Lagorio M., Cordon G., Iriel A., Romero J.M. Biophotonics, Fluorescence and Reflectance in Living Organisms." *Science Review from the end of the world.* 2(1): 18-41. 2020

McConnell I., Li G., Brudvig G.W. Thermal Conductivity of Cryogenic Insulation Systems. *Chemistry and Biology*. 17(5): 434-447. 2010

Mokbel K., Kodresko A., Ghazal H., Mokbel R., Trembley J., Jouhara H. Cryogenic Media in Biomedical Applications: Current Advances, Challenges, and Future Perspectives. *In Vivo*. 38(1):1–39. 2024

Nordrum A. The Era of Cheap Helium Is Over—and That's Already Causing Problems. *MIT Technology Review*. 2024

Ricci M, Benedetti E, Cruciani A, Hoang VL, Kalemi B, Naticchioni L, Orsini M, Pirro S, Puppo P, Rapagnani P. Cryogenic Facility for Prototyping ET-LF Payloads Using Conductive Cooling. *Galaxies*. 13(1): 1-12. 2025.

Sumitomo Heavy Industries, Ltd. *Instruction Manual for Helium Compressor CSW-71C*. Sumitomo Cryogenics of America, Inc., 2008

Sumitomo Heavy Industries, Ltd. *Operation Manual for SRDK Series CRYOCOOLER*. Sumitomo Cryogenics of America, Inc., 2003

Sumitomo Heavy Industries, Ltd., Cryocooler Technical Instruction Manual: RDK-205D. Sumitomo Cryogenics of America, Inc., 2005

Tan H, Li J., He M., Li J., Zhi D., Qin F., Zhang C. Global evolution of research on green energy and environmental technologies: A bibliometric study. *Journal of Environmental Management*. Vol. 297. 2021

Woodcraft A. Predicting the thermal conductivity of aluminium alloys in the cryogenic to room temperature range. Cryogenics. 45(6): 421-431. 2005

Zazubovich V., Ryszard J. Biophotonics of Photosynthesis. *Photonics: Scientific Foundations, Technology and Applications*. 4(1): 129–157. 2015